SERIES

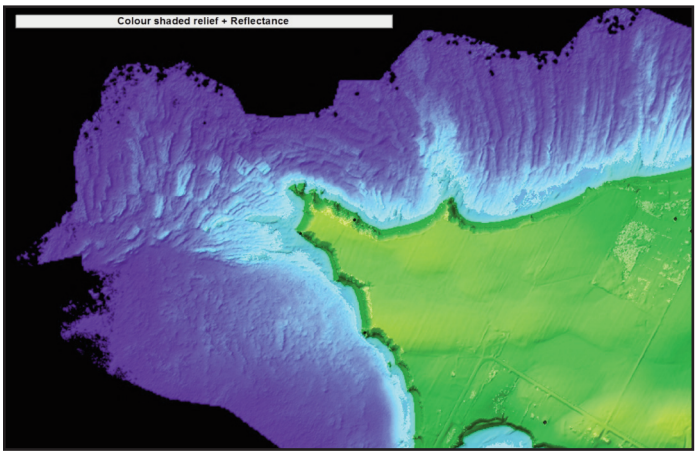

Remote Predictive Mapping 7. The Use of Topographic–Bathymetric Lidar to Enhance Geological Structural Mapping in Maritime Canada

Tim Webster, Kevin McGuigan, Nathan Crowell, Kate Collins and Candace MacDonald

Applied Geomatics Research Group
Nova Scotia Community College
Middleton, Nova Scotia, B0S 1M0, Canada
Email: tim.webster@nscc.ca

SUMMARY

An airborne topo-bathymetric lidar survey was conducted at Cape John, on the north shore of Nova Scotia, Canada, using the shallow water Leica AHAB Chiroptera II sensor. The survey revealed new bedrock features that were not discovered using previous mapping methods. A thick blanket of glacial till covers the bedrock on land, and outcrops are exposed only along the coastal cliffs and offshore reefs. The seamless land-seabed digital elevation model produced from the lidar survey revealed significant bedrock outcrop offshore where ocean currents have removed the glacial till, a significant finding that was hitherto hidden under the sea surface. Several reefs were identified offshore as well as a major fold structure where block faulting occurs along the limbs of the fold. The extension of the Malagash Mine Fault located ~10 km west of Cape John is proposed to explain the local folding and faulting visible in the submerged outcrops. The extension of this fault is partially visible on land, where it is obscured by glacial till, and its presence is supported by the orientation of submerged bedding and lineaments on both the south and north sides of Cape John. This paper demonstrates how near-shore high-resolution topography from bathymetric lidar can be used to enhance and refine geological mapping.

RÉSUMÉ

Un levé lidar topo-bathymétrique été réalisé à Cape John, sur la rive nord de la Nouvelle-Écosse, Canada, en utilisant un capteur Leci AHAB Chiroptera II. Ce levé a permis de repérer des affleurements que les méthodes de cartographie plus anciennes n'avaient pu détecter. Une épaisse couche de till glaciaire recouvre la roche en place sur le continent, et la roche affleure seulement le long des falaises côtières et des récifs côtiers. Le modèle numérique de dénivelé en continu terres et fonds marins obtenu par le levé lidar a révélé l'existence d'affleurement rocheux considérables au large des côtes, là où les courants océaniques ont emporté le till glaciaire, une découverte importante demeurée cachée sous la surface de la mer jusqu'alors. Plusieurs récifs ont été identifiés au large des côtes, ainsi qu'une structure de pli majeure, à l'endroit où se produit un morcellement en blocs le long des flancs du pli. Une extension de la faille de la mine Malagash situé ~ 10 km à l'ouest de Cape John est proposé pour expliquer les plis et les failles locaux visibles dans les affleurements submergés. L'extension de cette faille est partiellement visible sur la terre, voilée par le till, et sa présence est étayée par l'orientation de la stratification et des linéaments submergés tant du côté sud que nord de Cape John. Cet article montre comment la topographie haute résolution du lidar bathymétrique peut être utilisée pour améliorer et affiner la cartographie géologique.

Traduit par le Traducteur

INTRODUCTION

In this paper we present the results of offshore coastal mapping using airborne topo-bathymetric lidar at Cape John, Nova Scotia along the Northumberland Strait in the Gulf of St. Lawrence (Fig. 1). Traditional remote sensing mapping methods such as aerial photography and boat-based echo sounding used in the mapping of geological structures on the seabed can be difficult, time-consuming and expensive to locate. It is generally assumed that terrestrial outcrops extend underwater; Cape John is known to have outcrops along the coast but there

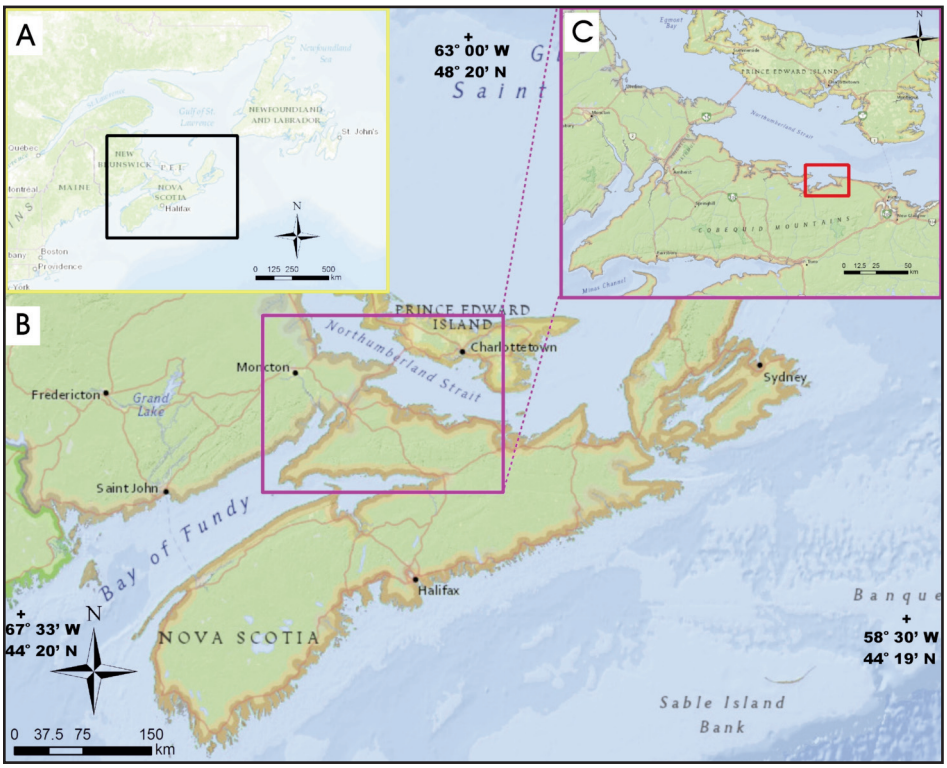

Figure 1. Overview of Atlantic Canada showing the location of the Cape John study site for the topo-bathymetric lidar survey. The black outline in A shows the location of B; C is the location of Figure 2, and the red rectangle in C outlines the area shown in Figure 3.

is little known about the distribution of geologic formations underwater, nor the fine details of the bathymetry, aside from a paper chart based on soundings from 1945 (Canadian Hydrographic Service 1945). At Cape John, the lack of outcrop on land, except for the coastal cliffs is a result of the deposition of glacial till during the last glacial period; however, the ability of an airborne sensor to accurately survey the nearshore bathymetry offers an opportunity to overcome the challenges of locating offshore exposures using traditional methods by providing detailed information on geologic structures that extend across the land-sea boundary.

Bathymetric data are traditionally collected using echo-sounding techniques in water depths greater than 10 m (Moustier and Matsumoto 1993; Clarke et al. 1996). However, these boat-based techniques are expensive and potentially hazardous in shallow water because of a limited survey field of view and the prospect of running aground. To overcome these issues, passive and active remote sensing techniques have been developed for shallow water bathymetry (Hedley and Mumby 2003; Jay and Guillaume 2014). Decker et al. (2011) have compared various methods for mapping bathymetry and water column properties from passive remote sensing. Hedley and Mumby (2003) presented a passive remote sensing technique whereby they modified a spectral unmixing method to calculate depth and substrate type from passive imagery. The technique requires pure spectral information of the substrate types very shallow and the water diffuse attenuation coefficients (Kd) for the site in the same spectral regions. Collecting Kd values during remote sensing data acquisition can be challenging, especially as these values change with conditions, such as increased turbidity or other water quality factors. Hedley and Mumby (2003) use realistic Kd values (0.15−0.25) along with random and actual spectra to test their spectral unmixing approach to mapping benthic cover, and found it to be insensitive to inaccuracies in depth estimation. Jay and Guillaume (2014) used a maximum likelihood estimation method for depth and water quality. Their method assumes that water column properties are similar for a group of at least 400 pixels having similar water clarity conditions, which is easier with high-resolution hyperspectral data.

Active remote sensing techniques for surveying depths utilize airborne topo-bathymetric lidar systems. Topo-bathymetric lidar works by emitting near-infrared (NIR) and green laser pulses from an aircraft and measuring the travel time of the pulses to and from the land, water surface, and seabed. The NIR laser pulse reflects off the land and sea surface, whereas the green laser pulse is refracted at the air-water interface, attenuated through the water column, and reflected from the seabed. Although topo-bathymetric lidar is a relatively new technology, it has been proven to be effective for mapping the fine detail of underwater bathymetry and geologic structures (Kennedy et al. 2008, 2014; Arifin and Kennedy 2011; Collin et al. 2011a, b, 2012; Coveney and Monteys 2011; Le Gall et al. 2014). The emerging uses of airborne laser bathymetry (ALB) for coastal research and coastal management are summarized in Brock and Purkis (2009). For example, Kennedy et al. (2014) used ALB (with the Laser Airborne Depth Sounder (LADS) Mk II sensor) and multibeam echo sounding to examine the erosion of granitic domes along the coast of southern Australia. Kennedy et al. (2014) concluded that coastal processes were removing debris and that the amount of erosion appeared to be related to the spacing of joints within the granite. They also calculated rugosity for the bathymetry and, in a series of offshore profiles, compared it to the jointing pattern present in the rock. Similarly, Le Gall et al. (2014) used lidar and multibeam bathymetry techniques to enhance their structural mapping of the Variscan basement off the coast of Brittany, France, allowing them to trace lineaments offshore and correlate them with geophysical maps. Covency and Monteys (2011) examined the integration of topographic lidar and ALB for coastal research along the Irish coastline. Others have studied the movement of offshore sediments, including Arifin and Kennedy (2011), who examined the evolution of large scale crescentic bars before and after hurricanes within the Gulf of Mexico, and Kennedy et al. (2008), who examined ephemeral sand waves in response

to hurricane forces in the surf zone off the coast of Florida. Collin et al. (2011a, b; 2012) used the Optech SHOALS system to survey a section of the coastal zone in the Gulf of St. Lawrence in Québec, focusing on benthic habitat.

Previous research has utilized large, deep-water lidar sensors such as the LADS Mk II, SHOALS and Hawkeye systems. A new generation of commercial, relatively lightweight, shallow-water sensors are now available, including the Leica AHAB Chiroptera II, Riegl VQ-820-G, and Optech Aquarius systems, allowing surveys to be conducted in smaller aircraft and at lower costs compared to sensors designed for deeper water. At the time of this study, the Chiroptera II was the only sensor that utilizes a NIR laser in combination with a green laser to map the sea surface; the VQ-820 and Aquarius systems rely only on a green laser for their operation. Wang et al. (2015) compared a variety of waveform-processing algorithms for single-wavelength lidar bathymetry systems and pointed out that the disadvantage of such systems is the lack of a NIR channel, leading to difficulties in extracting the water surface.

The Applied Geomatics Research Group at the Nova Scotia Community College recently acquired the Chiroptera II topo-bathymetric lidar sensor equipped with the Leica RCD30 medium-format 60 megapixel digital camera system capable of RGB (red-green-blue) and NIR image acquisition and motion compensation. We surveyed the Cape John area on September 26, 2014 and present here the methods used to process the lidar and seabed reflectance data, and to construct continuous elevation models, orthophotos, and a new interpretation of the structural geology based on the lidar data. Water clarity influences how deep the green laser will penetrate, and turbidity management is important for successful surveys. Webster et al. (in press) report on the influence of variable turbidity, and on advances in topo-bathymetric lidar data-processing techniques using multiple datasets collected around the Maritimes, including Cape John.

GEOLOGICAL SETTING

Cape John, Nova Scotia is located near the southern flank of the Maritimes (Carboniferous) Basin and is part of the Appalachian orogen (Fig. 1). The late Paleozoic evolution of the Appalachian orogen was profoundly influenced by post-accretionary motion along terrane boundaries (Williams and Hatcher 1982). The contact between the two most outboard terranes, the Avalon and Meguma terranes, can be traced across mainland Nova Scotia as the Minas Fault Zone (Cobequid−Chedabucto Fault System; Fig. 2). The Cobequid–Chedabucto Fault is interpreted to have had a history of recurrent movement that records important episodes of Late Paleozoic relative motion during the later tectonic phases of the Appalachian orogen (Keppie 1982; Mawer and White 1987; Murphy et al. 2011). Upper Devonian to Upper Carboniferous sedimentary rocks occur on both the Avalon and Meguma terranes and are generally considered to represent an overstep sequence across the boundary between the two terranes. The Cape John study area is located within the Cumberland Subbasin of the Maritimes Basin.

The Cumberland Subbasin is underlain by a thick accumulation of Lower Carboniferous to Lower Permian strata assigned to the Cumberland and Pictou groups in northwestern Nova Scotia and southeastern New Brunswick (Ryan and Boehner 1994) (Figs. 2, 3). It is bordered to the north by the Northumberland Strait and to the south by the Cobequid Highlands, which in turn is bordered to the south by the Cobequid−Chedabucto Fault (Fig. 2). The internal structure of the Cumberland Basin is generalized as a broad east- to northeast-trending synclinorium that is bounded by the parallel, diapiric, Claremont and Scotsburn anticlines; major synclines in the basin include the Tatamagouche and Wallace synclines (Ryan and Boehner 1994) (Figs. 2, 3). The Tatamagouche syncline and Claremont anticline (Figs. 2, 3) are genetically related and caused by tectonically driven diapirism (halotectonic; Ryan and Boehner 1994). The axis of the Tatamagouche Syncline traverses the Cape John study area, which is underlain by Upper Carboniferous rocks of the Pictou Group, consisting predominantly of continental clastic material deposited in fluvial and lacustrine settings (Gibling and Martel 1996) (Figs. 2, 3).The Pictou Group rests either disconformably or with angular unconformity over older Carboniferous strata of the Cumberland Group (Fig. 3). Younger rocks that may have overlain the Pictou Group are not preserved.

The major structural features of the region are the Cobequid−Chedabucto Fault and related faults such as the North Fault, which forms the boundary between the Cobequid Highlands and the Cumberland Basin (Ryan and Boehner 1994) (Fig. 2). The Cobequid−Chedabucto Fault is characterized by recurrent dextral strike-slip movement between the middle Devonian and early Permian (Mawer and White 1987; Webster and Murphy 1998; Murphy et al. 2011). Late Carboniferous activity along the fault zone was responsible for polyphase deformation (Nance 1987; Waldron et al. 1989) and the generation of local pull-apart basins (Bradley 1982; Yeo and Ruixiang 1987; Murphy and Keppie 1998). The North Fault has a complex history; it includes a series of splays that displaced Upper Carboniferous strata in the basin, whereas other units overlap the fault, whose trace has been interpreted through the use of remote sensing and geophysics (Ryan and Boehner 1994). The Malagash Mine Fault is west of the Cape John study area, on the west side of Amet Sound (Fig. 3). Faulting in the Malagash area is commonly associated with salt flow (Ryan and Boehner 1994). The Cape John Fault trends north-south at the end of the Cape John peninsula (Ryan and Boehner 1994) (Fig. 3). Fault movement here is predominantly normal dip-slip with a minor strike-slip component. Reidel shear sets adjacent to the Cape John Fault collectively indicate extensional stress oriented northwest-southeast, and associated with diapirism north of Cape John (Ryan and Boehner 1994). The Malagash−Claremont anticline has a normal south limb and a faulted north limb of overturned fault blocks having high-angle reverse or thrust geometry (Fig. 3). Movement on some of these faults is difficult to constrain and some may reflect later events such as Triassic rifting, which has been documented around the Bay of Fundy (Ryan and Boehner 1994; Webster et al. 2006).

http://www.dx.doi.org/10.12789/geocanj.2016.43.099

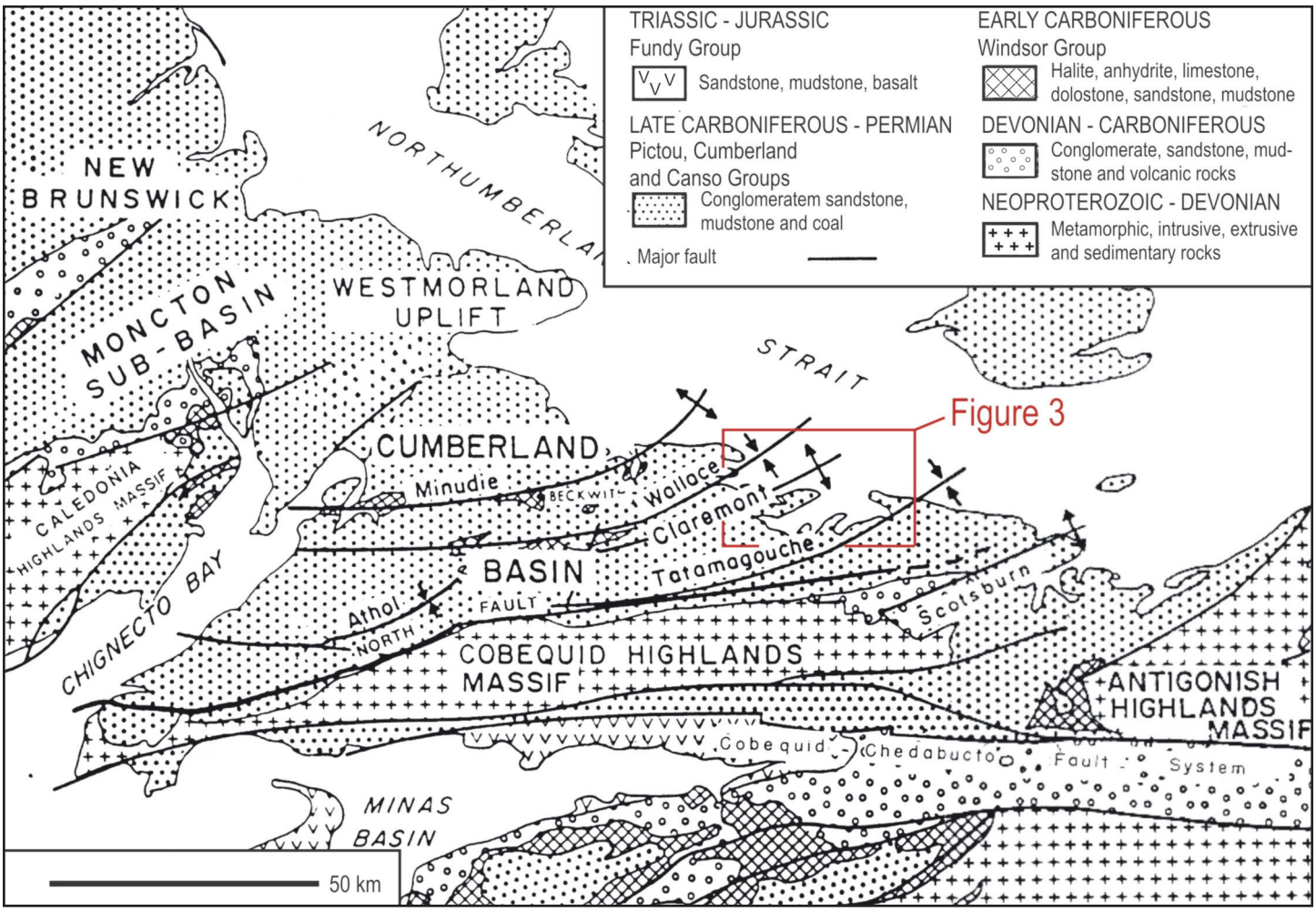

Figure 2. Regional structural setting and features of the Cumberland Basin, northern mainland Nova Scotia, after Ryan and Boehner (1994); the outline shows the extent of Figure 3.

The region was affected by fluctuations in Late Wisconsinan ice dynamics until ca. 12 ka (^{14}C yr) (Stea and Mott 1998). The earliest ice flows were eastward and southeastward from an Appalachian or Laurentide ice source ca. 75−40 ka (Caledonia ice flow phases 1A and 1B; Stea et al. 1998). The Hartlen Till was deposited by southeastward ice flow, and typically consists of 40% gravel, 40% sand, and 20% mud (silt and clay) (Lewis et al. 1998). The second major ice-flow was southward and southwestward from the Escuminac Ice Centre in the Prince Edward Island region (Escuminac ice flow phase 2, ca. 22−18 ka; Stea et al. 1998). The younger Lawrencetown Till (Stea et al. 1998) is a reddish muddy till unit that has a higher clay content than the Hartlen Till because of the incorporation of red Carboniferous sediment derived from Prince Edward Island, and typically consists of 20–30% gravel, 30–40% sand, and 30–50% mud (silt and clay) (Lewis et al. 1998). This deposit is locally known as the Eatonville−Hants Till. Ice then flowed northwestward and southward from the Scotian Ice divide across the axis of Nova Scotia (Scotian ice flow phase 3, ca. 18−15 ka; Stea et al. 1998). The study area is dominated by thick (ca. 3–5 m), red, clay-rich Lawrencetown Till.

METHODS

Topographic–Bathymetric Lidar System Specifications

The Chiroptera II topo-bathymetric lidar system incorporates a 1064 nm NIR laser for topographic returns and assisting in defining the water surface, and a green 515 nm laser for bathymetric returns (Fig. 4). The lasers utilize a Palmer scanner, which forms an elliptical pattern with angles of incidence of 14° forward and back and 20° to the sides of the flight track (Fig. 4). This scan pattern enables more returns from a single target from different angles, which reduces shadow effects and increases the number of points on vertical faces such as cliffs along the coast (Fig. 5). The elliptical scan pattern results in an increased likelihood that the target will be surveyed twice, from different angles a few seconds apart, and thus is less sensitive to ocean wave interaction whereby the air bubbles of a breaking wave will attenuate the green laser pulse (515 nm) and prevent penetration to the seabed.

The beam divergence of the topographic laser is 0.5 milliradians, and for the bathymetric laser is 3 milliradians. The topographic and bathymetric lasers have pulse repetition fre-

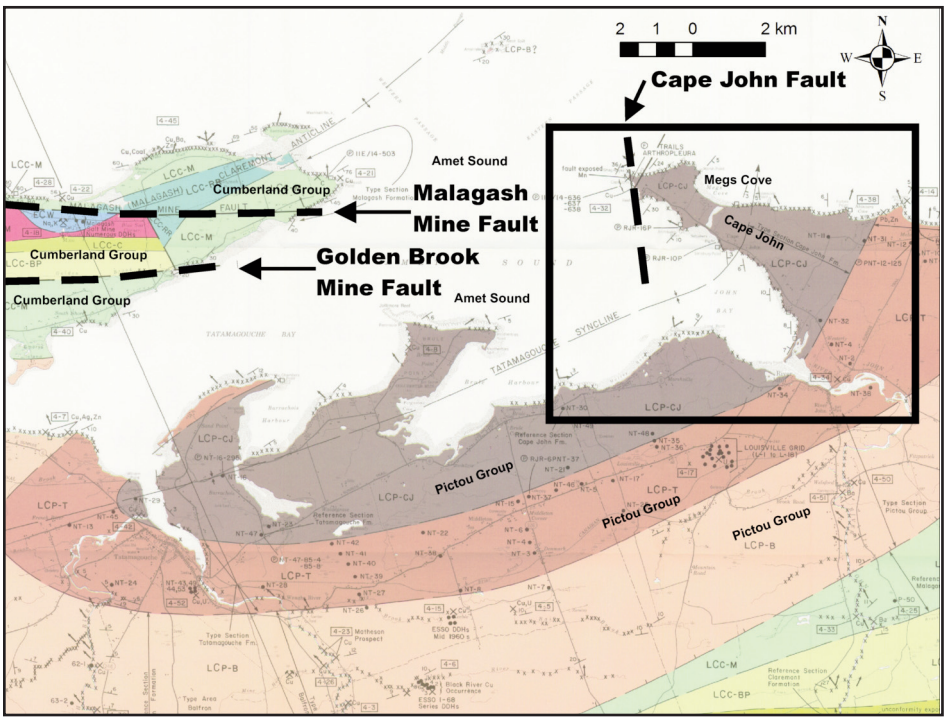

Figure 3. Geology of the Cumberland Basin, after Ryan and Boehner (1994). The black outline indicates the location of the topo-bathymetric lidar survey and the approximate extent of Figure 7. The Malagash Mine Fault, Golden Brook Fault and Cape John Fault are highlighted.

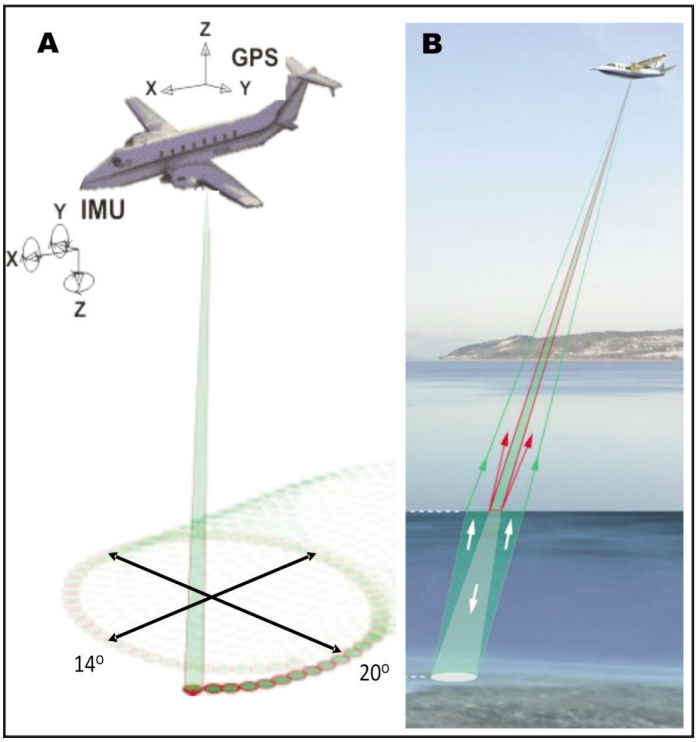

Figure 4. A. The elliptical scanning pattern of the Chiroptera II with GPS and Inertial Measurement Unit navigation system components. B. Illustration of the reflection of near-infrared topographic laser (red arrows) off the sea surface, and the green bathymetric laser (green and white arrows) penetrating the water column and reflecting off the sea bed. (Figures adapted from Leica Geosystems).

quencies up to 500 kHz and up to 35 kHz, respectively. The operational altitude of the bathymetric laser is between 400–600 m above ground level and for the topographic laser is up to 1600 m above ground level. The GPS has a sample rate of 1 Hz and the Inertial Measurement Unit has a sample rate of 200 Hz for positioning. The bathymetric accuracy of the bathymetric lidar is stated to be within 0.12 m at 2 standard deviations (95% confidence interval). The topographic laser is reported to have a ranging accuracy of 0.02 cm at 1 standard deviation (68% confidence interval) and a horizontal accuracy of 0.2 m at 1 standard deviation, not including GPS-Inertial Measurement Unit error. The system is equipped with a standard 5 megapixel RGB camera capable of exposures at 1 frame per second for quality assurance purposes, and is linked to the timing of the laser points. The Leica RCD30 camera collects co-aligned RGB+NIR motion-compensated photographs that can be orthorectified using direct georeferencing. The RCD30 is capable of exposures at 0.8 frames per second with a distortion-free lens having a focal length of 53 mm, and produces images of 6732 and 9000 pixels in the across- and along-track directions, respectively. The across-track field of view is 54°, which is slightly wider than the 40° across-track lidar field of view. At 400 m altitude the RCD30 produces imagery with a 5 cm pixel resolution.

The sensor was installed in a Beechcraft A90 King Air aircraft and calibration flights were conducted at altitudes of 400 m and 1000 m. The coastal bathymetric survey was acquired at an altitude of 400 m with 30% overlap between flight lines, and a flying speed of 55 m/s, resulting in a swath 291 m wide. Bathymetric lidar spot spacing was 1.56 m in the forward lateral direction and 0.78 m in the forward and backward scan direction, producing an average point density of 1.65 points/m^2. The green bathymetric laser spot diameter on the water surface is approximately 1.2 m at 400 m altitude, and the near-infrared topographic laser spot diameter is 0.2 m. Flight lines were planned parallel to the coastline, except for one additional line perpendicular to the coastline, intersecting the parallel lines. The specifications used for this survey were selected to maximize the resolution and point density of the lidar on land and submerged areas, and the photo resolution of 5 cm was a result of the flying height of 400 m above ground level. Specifications of the sensor and typical configurations can be found on the Leica Geosystems website (http://leica-geosystems.com/products/airborne-systems/bathymetric-hydrographic-sensors/leica-chiroptera-ii).

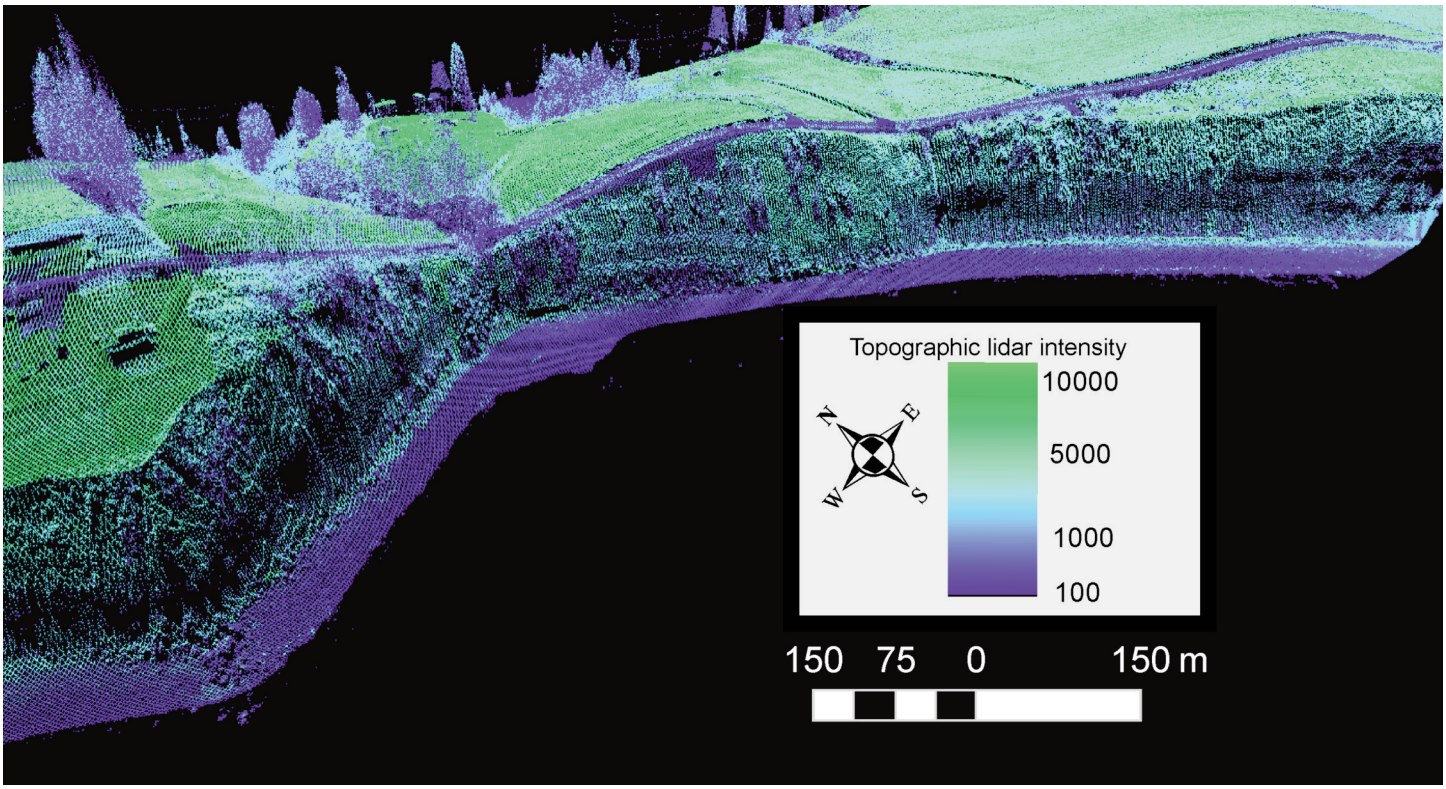

Figure 5. Example of dense point-spacing along coastal cliffs at Cape John, from the elliptical scan pattern of the Chiroptera II lidar. The colours in this perspective view represent differences in lidar intensity values from the topographic laser.

Lidar Survey

Depth penetration of the lidar sensor is limited by water clarity, as particles in the water column limit the laser's ability to travel through the water. The manufacturer suggests using a Secchi depth measurement to estimate the depth penetration of the laser under any given conditions. The Secchi depth is defined to be the depth at which a black and white Secchi disk is no longer visible as it is lowered into the water; clear water will have a large/deep Secchi depth, whereas turbid water will have a small/shallow Secchi depth. The Chiroptera II has a depth penetration limit of roughly 1.5 times the Secchi depth (Leica AHAB, personal communication 2014).

The shoreline at Cape John dominantly consists of sedimentary bedrock (red sandstone and mudstone) covered with a thick blanket of glacial till that is rich in red clay. Erosion of this material produces nearshore sediments that have a high clay content; this may cause increased turbidity when the sediments are mobilized by onshore wind and nearshore waves, preventing good laser penetration. Precipitation events can also cause runoff and increase turbidity. A weather station was installed at Cape John and the data measured there were broadcast through a cellular modem and used to monitor weather conditions remotely in order to conduct the survey during the clearest water possible.

The Cape John lidar survey was planned for September 24, 2014, but the weather data indicated that a significant storm event had occurred, accompanied by a drop in barometric pressure, wind speeds exceeding 40 km/hr from the northwest, and rainfall from September 18-22, causing the survey to be delayed. Following the storm, a high pressure system moved into the region, providing clear skies, so the survey was attempted on September 25. However, persistent winds of 20 to 40 km/hr during the time of the survey led to high turbidity levels and poor bathymetric laser returns, causing the survey to be aborted and delayed further. Good data were acquired during the second survey attempt on September 26 after suspended sediment had settled.

In-Situ Sampling

Ground-truth data acquisition is another important aspect of ALB data collection, especially since this was the first survey in the region with the Chiroptera II system. A Leica GS14 GPS system was used to set up a base station for the aircraft over a monument that was tied into the provincial High Precision Network. Real Time Kinematic GPS elevation validation checkpoints were collected along hard flat surfaces at the Cape John wharf to validate the topographic lidar, and Secchi depths were acquired along with underwater photographs of the seabed using a 1 m x 1 m quadrat (sampling area) to determine seabed cover. A Reson T-20 multibeam system was deployed in October after the ALB survey was completed so that additional depth validation points could be acquired. The vessel was also equipped with an MDL Dynascan mobile laser scanner that has a dual survey grade GPS antenna configuration for improved heading measurements and an Inertial Measurement Unit for direct georeferencing. The Dynascan

supplied the real-time navigational corrections for the multibeam, and data from both sensors were acquired using QINSy™ acquisition software.

Lidar Processing

Once the aircraft GPS-Inertial Measurement Unit trajectory was processed utilizing the GPS base station, the navigation data were linked to the laser returns and georeferenced using Lidar Survey Studio™ (LSS). The lidar data were then processed within LSS, which classified the laser waveforms into discrete points (the LSS software computes the water surface from the lidar returns of both the topographic and bathymetric lasers). In addition to classifying points as land, water surface, or bathymetry, the system also computed a modelled water surface that ensured the entire surface area of water was covered, regardless of the original lidar point density. Threshold parameters were set within LSS to classify the bathymetry points from the waveforms. The point cloud can be viewed in cross-section or in a perspective view, allowing the land to be separated from the bathymetry points (Fig. 6). Once the waveforms were processed, the resultant points were displayed using a variety of attributes (flight line, elevation, intensity) within LSS, and the waveform examined with the 5 megapixel quality assurance airphoto, which was linked to the lidar scans. LAS (an open standard file format for the interchange of lidar data) version 1.2 files were exported from LSS for further classification and filtering in TerraScan™, where the separation of bathymetric points and noise was refined. As an example of the variation in files and volume of data, the raw waveform data are stored in 200 MB files, reduced to 70 MB files when converted to discrete point files in LAS format, and further reduced to 3 MB as a 2 m-resolution raster grid.

The refined, classified LAS files were then read into an ArcGIS™ LAS dataset, and Python™ scripts were written to produce a variety of raster surfaces at a 2 m spatial sampling interval. Three main data products are derived from the lidar point cloud. The first two are based on the elevation and include: 1) the digital surface model (DSM), which incorporates valid lidar returns from vegetation, buildings, ground and bathymetry returns; and 2) the digital elevation model (DEM), which incorporates ground returns above and below the water line. The elevation attribute of the lidar point cloud is relative to the WGS84 ellipsoid, since the point reference is based on the GPS aircraft trajectory. However, once the surface models (DSM and DEM) were constructed using different combinations of the point class elevations, the data were converted to orthometric heights relative to the Canadian Geodetic Vertical Datum of 1928. The geoid-ellipsoid separation model, HT2, available from Natural Resources Canada, was used for this conversion of the surface models.

The third data product is the amplitude of the lidar returns of the bathymetric laser. The amplitude values were depth-normalized by taking samples of the amplitude values of a common cover type (such as sand) over depth ranges, and using these data to establish a relationship between depth and the amplitude value; the inverse of this relationship was used to depth-normalize the amplitude data. The amplitude or reflectance of the green laser can be interpreted for seabed cover, e.g. sand, submerged aquatic vegetation, rock or potential bedrock structures. In order to easily interpret the lidar surface models, colour shaded relief models were constructed from the DSM and DEM for the study site. Figure 7 shows a DEM of the 2014 topo-bathymetric lidar survey combined with topographic lidar collected in 2006 and 2007. The missing strips of data in the southern portion of the study area (Fig. 7) occurred because fog was present during this part of the survey, which caused the lasers to reflect back towards the aircraft at close range, triggering a safety shut off. This happened on a few flight lines (Fig. 7) before it was resolved and continuous data were re-acquired.

RESULTS

Elevation Validation

GPS checkpoints collected at the end of the Cape John wharf were compared to the topographic lidar-derived elevation surface (DEM). The mean difference between the GPS elevation and the DEM was –0.02 m, with a standard deviation of 0.04 m from 13 checkpoints. The topographic sensor was well within the manufacturer's specifications of 15 cm vertical accuracy. Rough weather and technical challenges limited the quantity of depth validation data collected during the multibeam survey; therefore, more depth validation studies are planned for the future. The validation of the depths at Cape John was accomplished by qualitatively comparing the multibeam echosounder depths to the lidar bathymetry points where overlap exists. Results indicate that the lidar bathymetric points match the multibeam points within the 15 cm specification of the Chiroptera II.

Geological Interpretation

The 2014 topo-bathymetric lidar data reveal that ocean currents have eroded the glacial till cover offshore and exposed the bedrock geology around Cape John (Fig. 8). These data allow the coastal outcrops to be traced laterally and more details on the structural geology to be interpreted. The offshore structures thus revealed include bedding planes of the Cape John Formation, which generally strike northeast but curve to the north-south toward the west end of Cape John (Fig. 8B). Ryan and Boehner (1994) mapped north-northeast- and north-south-trending faults at the end of Cape John (Fig. 9); the north-northeast trending fault corresponds to where the 2014 lidar bathymetry begins to show more intense deformation (Fig. 8). Bedding appears to be folded and faulted in an arcuate shape around the point at Cape John, changing from a northeast trend to an east-west trend, then back to a northeast trend farther west. Large blocks are dextrally offset by faults, which also appear to be folded (Fig. 8B). The elevation and apparent deformation of the submerged outcrop diminishes south of the point on the west side of Cape John (Fig. 8B). Near the wharf south of Cape John bedding trends east-west, parallel to two major onshore lineaments that are expressed as subtle depressions and wetland locations (Fig. 8B, C). The lineaments are broad, low-lying, and may have been preferentially

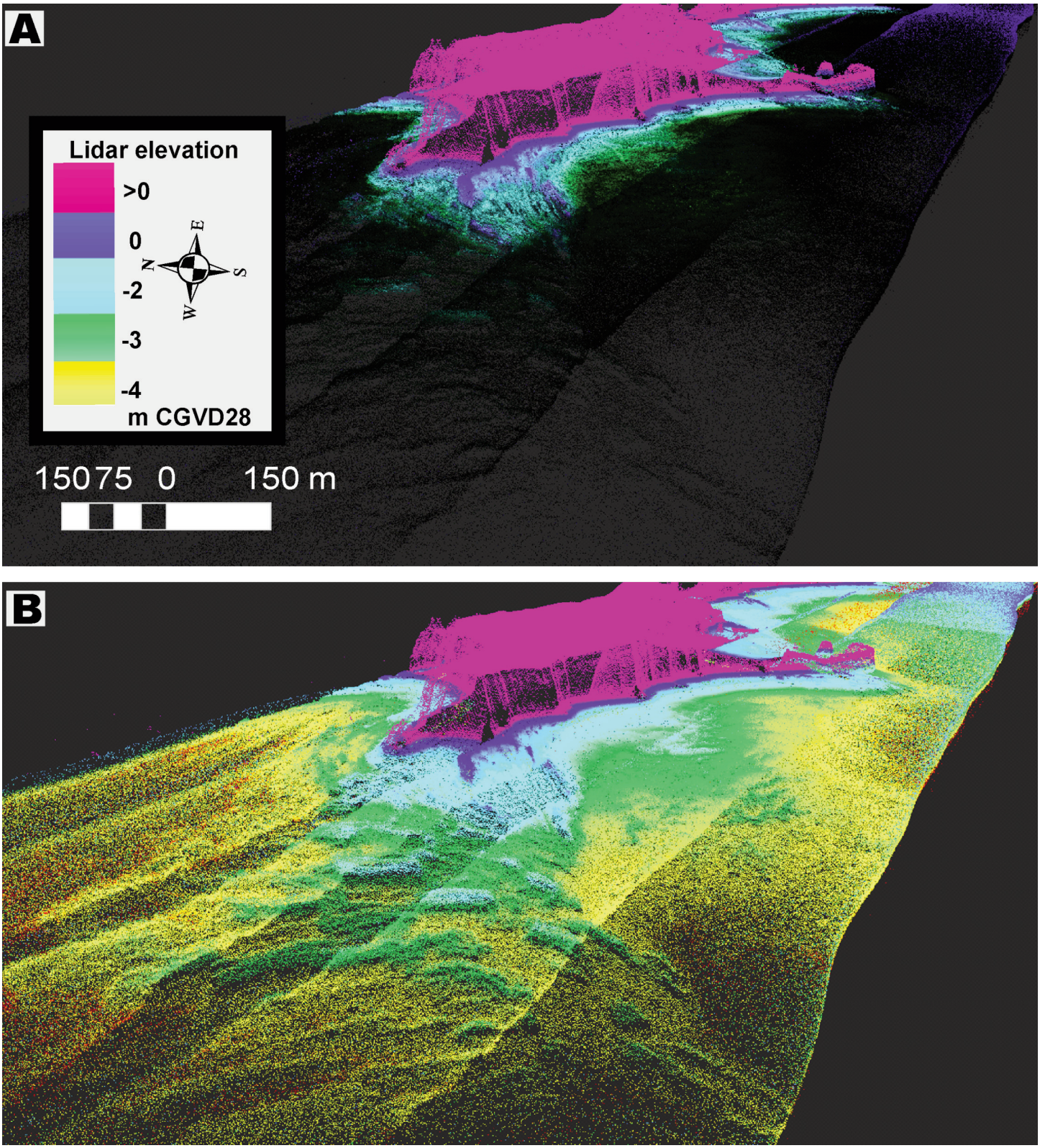

Figure 6. Point clouds for Cape John, colour-coded for elevation. A. Perspective view of the topographic laser points highlighting the exposed land. B. Perspective view of the combined topo-bathymetric lasers; the green features represent submerged, folded fault blocks.

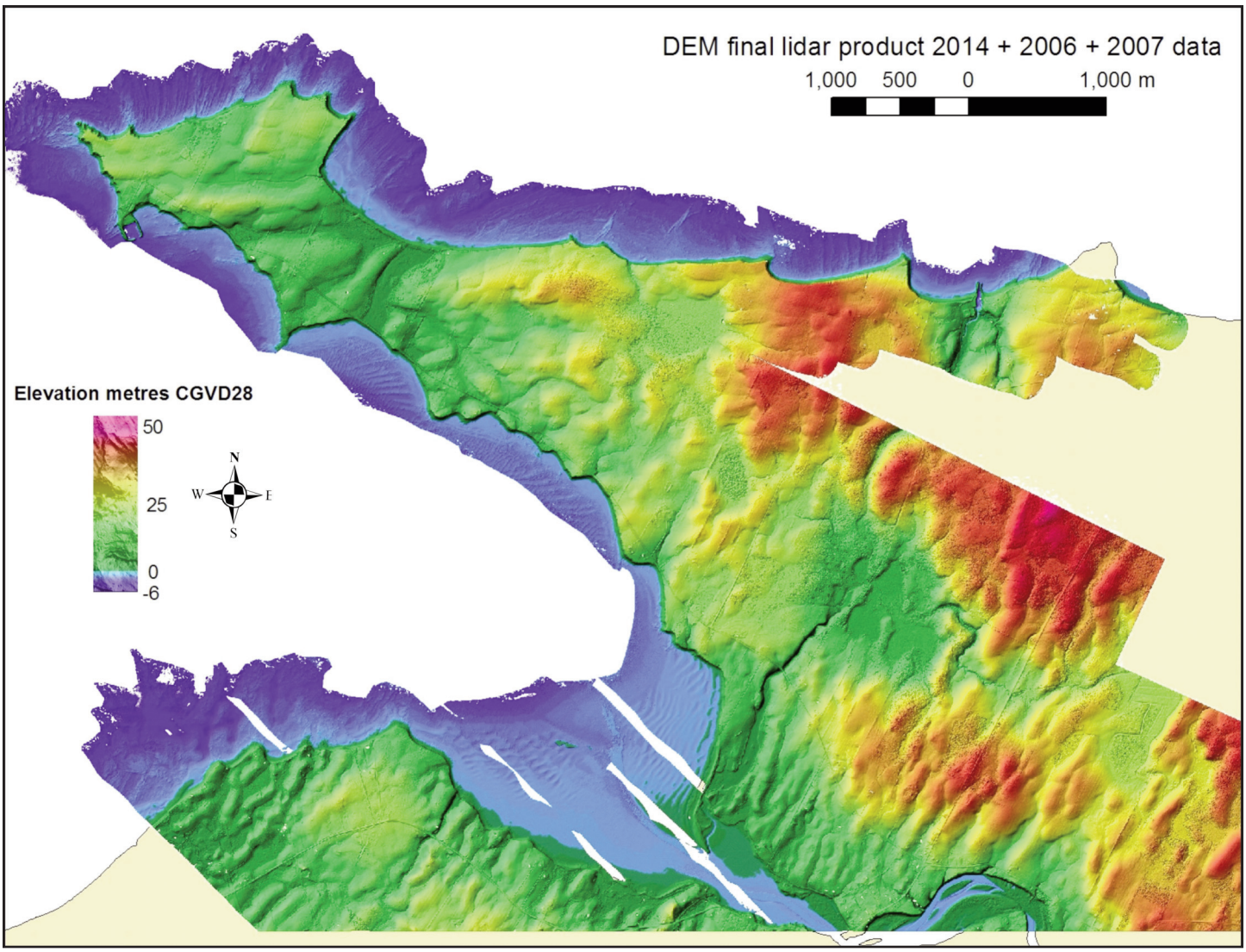

Figure 7. Colour shaded relief of topo-bathymetric lidar Digital Elevation Model for Cape John, Nova Scotia.

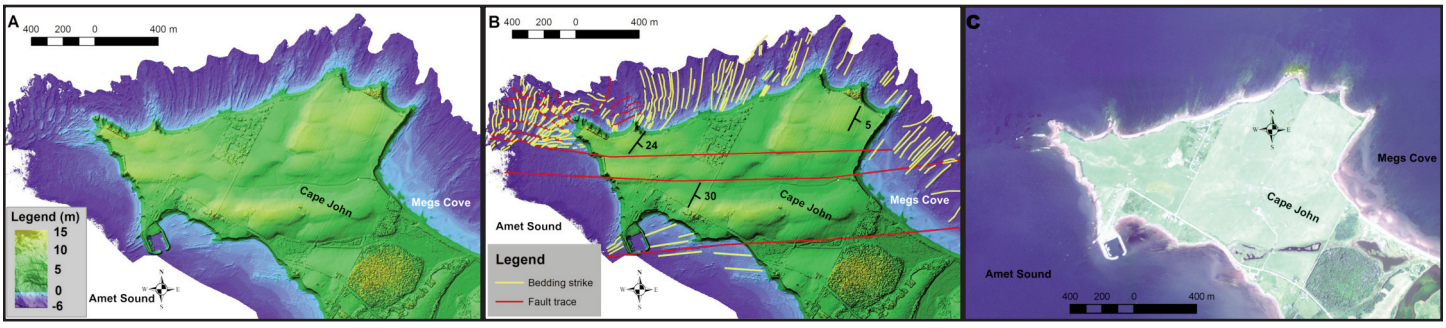

Figure 8. A. Close-up of offshore structural geology revealed by topo-bathymetric lidar Digital Surface Model (DSM). B. Map of lidar DSM with the geological interpretation of bedding attitude (yellow lines) and faults (red lines). Bedding symbols are from Ryan and Boehner (1994). C. Example of a low tide Worldview 2 image true colour composite, September 2010 (image copyright © DigitalGlobe).

eroded by glaciers. These lineaments are evident on a Worldview 2 satellite image acquired at low tide in September 2010, which was examined and interpreted for lineaments and exposed and submerged outcrop (Fig. 8C). However, the satellite image contains little information on exposed or submerged outcrops compared to what is visible in the lidar DEM (Fig. 8A, B). The lineaments are aligned with breaks in the strike of the offshore bedding planes and also with extrapolated positions of the Malagash Mine and Golden Brook faults, mapped less than 10 km to the west across Amet Sound (Fig. 9A). The

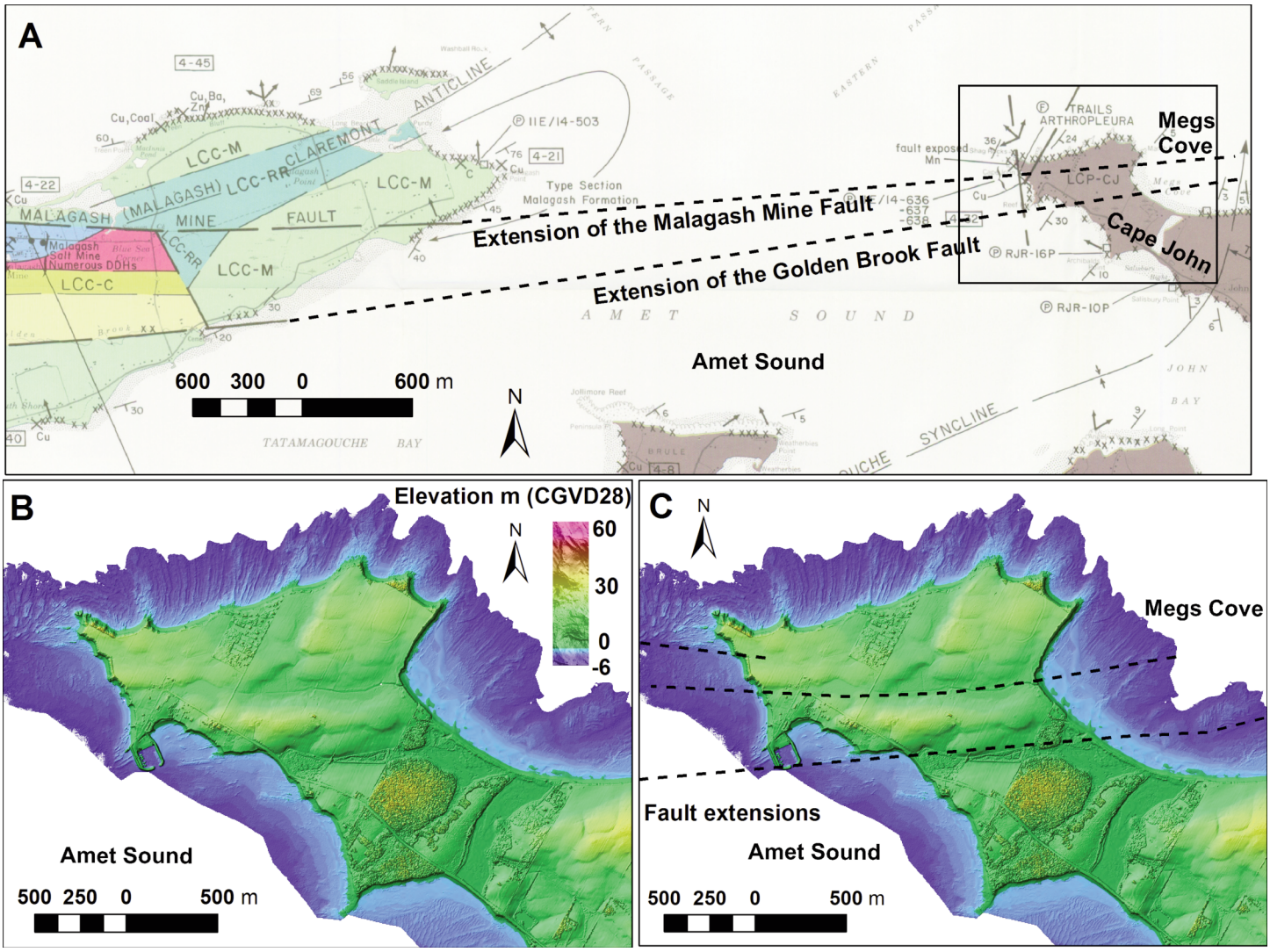

Figure 9. A. Projection of the Malagash Mine and Golden Brook faults to Cape John, with lidar map location outlined in black. Geology is from Ryan and Boehner (1994). B. Lidar Digital Surface Model (DSM) of the area enclosed by the black rectangle in A. C. Lidar DSM with interpreted fault extensions (black dashed lines) following the onshore lineaments.

extrapolated faults also line up with lineaments identified offshore on the east side of Cape John (Fig. 9), separating north-northeast-striking beds on the west side of Megs Cove to the northwest (Fig. 9).

CONCLUSIONS

The topo-bathymetric lidar provides greater detail both on the land and in the submerged nearshore compared to previously available information from geological and hydrographic surveys. Conventional topographic lidar surveys completed between 2006 and 2011 reveal that the land is covered by a blanket of glacial till, and that landforms appear to be dominated by the late movement of ice (Fig. 7). However, because the topographic NIR laser does not penetrate the water column, no information of the submerged terrain is available from these older surveys. The topo-bathymetric lidar data also provide far greater detail to a depth of 6 m compared to a hydrographic chart of the area that was compiled in 1945 (Canadian Hydrographic Service 1945) (Fig. 8). Bedrock geology can only be mapped along the coast, and is only accessible during low tide or by boat, therefore the interpretation of the structural geology is limited by what is seen at the coastal sections. Conversely, the topo-bathymetric lidar study identified nearshore lineaments representing bedding planes and possible faults, which we have correlated with known onshore faults and lineaments. This interpretation has resulted in extending several faults, such as the Malagash Mines and Golden Brook faults, farther east to Cape John, where they explain some of the nearshore deformation in that area. In Brittany, Le Gall et al. (2014) similarly used lidar and multibeam to enhance their structural mapping of the offshore Variscan basement, allowing them to trace lineaments, correlate them with geophysics, and interpret the deformation. Unfortunately, the regional geophysics, including magnetics, in the Cape John area is of low resolution and does not reveal any structural details.

This paper provides an example showing how ALB data can be used to examine and interpret structural geology and to extend onshore mapping into the nearshore. The study has revealed a significant amount of exposed outcrop in the nearshore. The glacial till, which obscures outcrop on land, has been eroded in the nearshore, clearly revealing bedding planes in the high-resolution elevation model derived from ALB. The structural details that can be interpreted from the nearshore bathymetry far exceed the details that can be seen on land, which is covered by a thick blanket of glacial till from the Laurentian ice sheet. Because of the till blanket, the only available outcrop on land is along the coast, which does not provide sufficient lateral extent to allow the full complexity of the geological structures within the study area to be identified. The results of previous mapping, combined with the newly interpreted nearshore bathymetry, have been used to extrapolate several faults and link onshore wetlands and marshes with offshore breaks in the attitude of bedding planes. These techniques can be applied elsewhere and may, for example, allow the extension of known mineral deposits to be traced into the nearshore or, as demonstrated in this study, improve our geological maps and understanding of local tectonics.

ACKNOWLEDGEMENTS

The Applied Geomatics Research Group at Nova Scotia Community College would like to thank the Canada Foundation for Innovation (CFI) and our CFI project partner, Leading Edge Geomatics (LEG) who assisted in the operation of the survey and arranging the aircraft for the sensor. Staff from Leica AHAB and Leica Geosystems were on site for training and assisted us with the installation, calibration and initial processing of the data. We would like to thank the following project partners who assisted in funding the equipment and processing of the data for this paper: Nova Scotia Research Innovative Trust, Atlantic Canada Opportunities Agency, GeoNova, Nova Scotia government departments: Natural Resources, Fisheries and Aquaculture, Agriculture and Inland Waters, as well as Federal Government departments: Public Works Government Services Canada, Fisheries and Oceans Canada (Gulf Region and Maritimes Region), and the Natural Science and Engineering Research Council. Additionally, the authors would like to thank the reviewers of this manuscript, Dr. Brendan Murphy and Dr. Jeff Harris. We would also like to thank the copyeditor, Reginald Wilson, for his helpful comments on the manuscript.

REFERENCES

Arifin, R.R., and Kennedy, A.B., 2011, The evolution of large scale crescentic bars on the northern Gulf of Mexico coast: Marine Geology, v. 285, p. 46–58, http://dx.doi.org/10.1016/j.margeo.2011.04.003.

Bradley, D.C., 1982, Subsidence in Late Paleozoic basins in the northern Appalachians: Tectonics, v. 1, p. 107–123, http://dx.doi.org/10.1029/TC001i001p00107.

Brock, J.C., and Purkis, S.J., 2009, The emerging role of LiDAR Remote Sensing in coastal research and resource management: Journal of Coastal Research, Special Issue 53, p. 1–5, http://dx.doi.org/10.2112/SI53-001.1.

Calder, J.H., Gillis, K.S., MacNeil, D.J., Naylor, R.D., and Watkins Campbell, N., 1993, One of the greatest treasures – the geology and history of coal in Nova Scotia: Nova Scotia Department of Natural Resources Mineral Resources Branch Information Circular ME 25, 50 p.

Canadian Hydrographic Service, 1945, Amet Sound. [Chart CHS4497]: Government of Canada, Fisheries and Oceans Canada, Ottawa, scale 1:28850.

Clarke, J.E.H., Mayer, L.A., and Wells, D.E., 1996, Shallow-water imaging multibeam sonars: A new tool for investigating seafloor processes in the coastal zone and on the continental shelf: Marine Geophysical Researches, v. 18, p. 607–629, http://dx.doi.org/10.1007/BF00313877.

Collin, A., Archambault, P., and Long, B., 2011a, Predicting species diversity of benthic communities within turbid nearshore using full-waveform bathymetric LiDAR and machine learners: PloS ONE, v. 6, e21265, http://dx.doi.org/10.1371/journal.pone.0021265.

Collin, A., Long, B., and Archambault, P., 2011b, Benthic classifications using bathymetric LIDAR waveforms and integration of local spatial statistics and textural features: Journal of Coastal Research, p. 86–98, http://dx.doi.org/10.2112/SI_62_9.

Collin, A., Long, B., and Archambault, P., 2012, Merging land-marine realms: Spatial patterns of seamless coastal habitats using a multispectral LiDAR: Remote Sensing of Environment, v. 123, p. 390–399, http://dx.doi.org/10.1016/j.rse.2012.03.015.

Coveney, S., and Monteys, X., 2011, Integration potential of INFOMAR Airborne LIDAR bathymetry with external onshore LIDAR data sets: Journal of Coastal Research, p. 19–29, http://dx.doi.org/10.2112/SI_62_3.

Dekker, A.G., Phinn, S.R., Anstee, J., Bissett, P., Brando, V.E., Casey, B., Fearns, P., Hedley, J., Klonowski, W., Lee, Z.P., Lynch, M., Lyons, M., Mobley, C., and Roelfsema, C., 2011, Intercomparison of shallow water bathymetry, hydro-optics, and benthos mapping techniques in Australian and Caribbean coastal environments: Limnology and Oceanography: Methods, v. 9, p. 396–425, http://dx.doi.org/10.4319/lom.2011.9.396.

de Moustier, C., and Matsumoto, H., 1993, Seafloor acoustic remote sensing with multibeam echo-sounders and bathymetric sidescan sonar systems: Marine Geophysical Researches, v. 15, p. 27–42, http://dx.doi.org/10.1007/BF01204150.

Devanney, M., and Doyle, S., 1989, Nova Scotia Gold: Nova Scotia Department of Mines and Energy Information Circular 4, 7 p.

Hedley, J.D., and Mumby, P.J., 2003, A remote sensing method for resolving depth and subpixel composition of aquatic benthos: Limnology and Oceanography, v. 48, p. 480–488, http://dx.doi.org/10.4319/lo.2003.48.1_part_2.0480.

Jay, S., and Guillaume, M., 2014, A novel maximum likelihood based method for mapping depth and water quality from hyperspectral remote-sensing data: Remote Sensing of Environment, v. 147, p. 121–132, http://dx.doi.org/10.1016/j.rse.2014.01.026.

Kennedy, A.B., Slatton, K.C., Hsu, T.-J., Starek, M.J., and Kampa, K., 2008, Ephemeral sand waves in the hurricane surf zone: Marine Geology, v. 250, p. 276–280, http://dx.doi.org/10.1016/j.margeo.2008.01.015.

Kennedy, D.M., Ierodiaconou, D., and Schimel, A., 2014, Granitic coastal geomorphology: applying integrated terrestrial and bathymetric LiDAR with multibeam sonar to examine coastal landscape evolution: Earth Surface Processes and Landforms, v. 39, p. 1663–1674, http://dx.doi.org/10.1002/esp.3615.

Keppie, J.D., 1982, The Minas Geofracture, *in* St. Julien, P., and Beland, J., *eds.,* Major structural zones and faults of the northern Appalachians: Geological Association of Canada, Special Paper 24, p. 263–280.

Le Gall, B., Authemayou, C., Ehrhold, A., Paquette, J.-L., Bussien, D., Chazot, G., Aouizerat, A., and Pastol, Y., 2014, LiDAR offshore structural mapping and U/Pb zircon/monazite dating of Variscan strain in the Leon metamorphic domain, NW Brittany: Tectonophysics, v. 630, p. 236–250, http://dx.doi.org/10.1016/j.tecto.2014.05.026.

Lewis, C.F.M., Taylor, B.B., Stea, R.R., Fader, G.B.J., Horne, R.J., MacNeill, S.G., and Moore, J.G., 1998, Earth Science and Engineering: Urban development in the Metropolitan Halifax Region, *in* Karrow, P.F., and White, O.L., *eds.*, Urban Geology of Canadian Cities: Geological Association of Canada Special Paper 42, p. 409–444.

Martel, A.T., and Gibling, M., 1996, Stratigraphy and tectonic history of the Upper Devonian to Lower Carboniferous Horton Bluff Formation, Nova Scotia: Atlantic Geology, v. 32, p. 13–38.

Mawer, C.K., and White, J.C., 1987, Sense of displacement on the Cobequid–Chedabucto fault system, Nova Scotia, Canada: Canadian Journal of Earth Sciences, v. 24, p. 217–223, http://dx.doi.org/10.1139/e87-024.

Murphy, J.B., and Keppie, J.D., 1998, Late Devonian palinspastic reconstruction of the Avalon-Meguma terrane boundary: implications for terrane accretion and basin development in the Appalachian orogen: Tectonophysics, v. 284, p. 221–231, http://dx.doi.org/10.1016/S0040-1951(97)00177-7.

Murphy, J.B., Waldron, J.W.F., Kontak, D.J., Pe-Piper, G., and Piper, D.J.W., 2011, Minas Fault Zone: Late Paleozoic history of an intra-continental orogenic transform fault in the Canadian Appalachians: Journal of Structural Geology, v. 33, p. 312–328, http://dx.doi.org/10.1016/j.jsg.2010.11.012.

Nance, R.D., 1987, Dextral transpression and Late Carboniferous sedimentation in the Fundy coastal zone of southern New Brunswick: CSPG Special Publication, Memoir 12, p. 363–377.

Ryan, R.J., and Boehner, R.C., 1994, Geology of the Cumberland Basin, Cumberland, Colchester and Pictou Counties, Nova Scotia: Nova Scotia Department of Natural Resources Mineral Resources Branch Memoir ME 10, 213 p.

Stea, R.R., and Mott, R.J., 1998, Deglaciation of Nova Scotia: Stratigraphy and chronology of lake sediment cores and buried organic sections: Geographie physique et Quaternaire, v. 50, p. 3–21, http://dx.doi.org/10.7202/004871ar.

Stea, R.R., Piper, D.J.W., Fader, G.B.J., and Boyd, R., 1998, Wisconsinan glacial and sea-level history of Maritime Canada and the adjacent continental shelf: A cor-

relation of land and sea events: Geological Society of America Bulletin, v. 110, p. 821–845, http://dx.doi.org/10.1130/0016-7606(1998)110<0821:WGASLH>2.3.CO;2.

Waldron, J.W.F., Piper, D.J.W., and Pe-Piper, G., 1989, Deformation of the Cape Chignecto Pluton, Cobequid Highlands, Nova Scotia: thrusting at the Meguma–Avalon boundary: Atlantic Geology, v. 25, p. 51–62, http://dx.doi.org/10.4138/1670.

Wang Chisheng, Li Qingquan, Liu Yanxiong, Wu Guofeng, Liu Peng, and Ding Xiaoli, 2015, A comparison of waveform processing algorithms for single-wavelength LiDAR bathymetry: ISPRS Journal of Photogrammetry and Remote Sensing, v. 101, p. 22–35, http://dx.doi.org/10.1016/j.isprsjprs.2014.11.005.

Webster, T.L., Murphy, J.B., and Barr, 1998, Anatomy of a terrane boundary: an integrated structural, geographic information system, and remote sensing study of the late Paleozoic Avalon-Meguma terrane boundary, mainland Nova Scotia, Canada: Canadian Journal of Earth Sciences, v. 35, p. 787–801, http://dx.doi.org/10.1139/cjes-35-7-787.

Webster, T.L., Murphy, J.B., and Gosse, J.C., 2006, Mapping subtle structures with light detection and ranging (LIDAR): flow units and phreatomagmatic rootless cones in the North Mountain Basalt, Nova Scotia: Canadian Journal of Earth Sciences, v. 43, p. 157–176, http://dx.doi.org/10.1139/e05-099.

Webster, T., McGuigan, K., Crowell, N., Collins, K., and MacDonald, C., in press, Optimization of data collection and refinement of post-processing techniques for Maritime Canada's first shallow water topographic-bathymetric lidar survey: Journal of Coastal Research, Special issue on Advances in Topo-Bathymetric lidar.

Williams, H., and Hatcher Jr., R.D., 1982, Suspect terranes and accretionary history of the Appalachian orogen: Geology, v. 10, p. 530–536, http://dx.doi.org/10.1130/0091-7613(1982)10<530:STAAHO>2.0.CO;2.

Yeo, G.M., and Ruixiang, G., 1987, Stellarton Graben: An Upper Carboniferous pull-apart basin in northern Nova Scotia: CSPG Special Publications, Memoir 12, p. 299–309.

Received January 2016
Accepted as revised May 2016
First published on the web May 2016